

## EXPERIMENTAL AND NUMERICAL ANALYSIS OF THE DOE REFERENCE MODEL 1 HORIZONTAL AXIS HYDROKINETIC TURBINE

**Teymour Javaherchi**

University of Washington - NNMREC  
Seattle, WA, USA

**Nick Stelzenmuller**

University of Washington - NNMREC  
Seattle, WA, USA

**Alberto Aliseda\***

University of Washington - NNMREC  
Seattle, WA, USA

### ABSTRACT

We present experimental and numerical simulation studies of a Horizontal Axis Hydrokinetic Turbine (HAHT) based on the DOE Reference Model 1. The performance and wake of a small array of three turbines was analyzed with measurements conducted on a 45:1 scale physical model of the DOE RM1 rotor. The influence of the Reynolds number dissimilarity between the laboratory model and the full scale is described. The details of the rotor flow field and wake evolution are analyzed from numerical solution of the RANS equations solved around a computational model of the full scale geometry. The influence of turbulent closure models is considered, as is the use of high resolution simulations in lower fidelity models for fast turn around, low computational cost, numerical design efforts.

### INTRODUCTION

Marine HydroKinetic (MHK) turbines are in an early stage of development, with many unanswered questions regarding their performance, optimization, and environmental effects. Many previous studies [1,2,3,?,?] have addressed these questions by either numerical simulation or laboratory experiments using a wide range of turbine geometries. The creation of the DOE Reference Model 1 (DOE RM 1) reference turbine geometry allows for direct comparison of results and analysis from different research groups. The numerical simulations and experimental results presented here use this reference model to study the performance and wake hydrodynamics of this horizontal axis hydrokinetic turbine (HAHT).

Laboratory-scale testing of horizontal axis hydrokinetic turbines (HAHT) is used to validate numerical models and gain in-

sight into the performance and wake dynamics of HAHT. Recirculating flumes and towing tanks are used for these tests, with measurements of the torque produced at the shaft, the rotational speed, and the drag (or thrust) force on the HAHT, as well as flow velocity characteristics. Many studies [?, ?, ?] have been performed to characterize the performance of single HAHT with various rotor geometries. Interactions between multiple HAHT have been investigated recently: Mycek et al. [?] measured HAHT performance and wake interaction for two HAHT in a coaxial configuration, and Stallard et. al [?] studied the wake interactions for multiple HAHT arranged laterally. Mycek et al. found that the overall array efficiency could be increased by operating the upstream turbine at a non-optimum tip speed ratio, which has implications for “tuning” of arrays for greater efficiency. The experimental results presented here use three HAHT, in configurations that vary both streamwise and lateral spacing.

On the area of numerical modeling the NREL recently proposed a new turbine design, officially named the DOE Reference Model 1 (DOE RM 1), as an open source design for HAHT that researchers can use to benchmark their studies. Lawson et al. [3] have performed numerical analysis on this reference model using RANS simulation. They investigated the effect of mesh resolution on numerical modeling of the DOE RM 1 and characterized the turbine performance using both steady and transient models. Lawson et al. reported a good agreement between unsteady and steady simulations for the optimal operating conditions ( $TSR = 6.3$  and  $\theta_p = 0^\circ$ ), where the flow is fully attached to the turbine blade. However, they mention that for the other operating conditions unsteady models might be better choice to provide more accurate results for the flow field and turbine performance characterization. They mentioned that including other parts of the turbines such as the tower and the nacelle and investigation of more realistic boundary conditions are parts of their future work.

---

\*Corresponding Author: aaliseda@uw.edu

Another recent study on numerical modeling of HAHT has been carried out at Saint Anthony Falls laboratory [?] . Kang et al. performed an LES simulation on the Gen4 KHPS turbine developed by Verdant Power for the Roosevelt Island Tidal Energy (RITE) project in the East River in New York. They investigated flow field behavior in the near wake of this turbine, the grid resolution effect on the numerical results and the coherent vortex structures shed into the turbine’s near wake. Kang et al. concluded that the pressure field near the turbine blades is not significantly affected by the structural parts of the turbine (i.e. pylon, nacelle, etc.). They mentioned that this observation suggests that the simulation of the isolated rotor can be sufficient for predicting the power of this HAHT design. Kang et al. validate their numerical model via the available field data and plan to use their validated numerical tool to investigate site specific variations such as complex topography of the field site and the shear velocity profile on the performance of this turbine.

Similar to the above-cited studies on the MHK technology this paper investigates different aspects of HAHTs via numerical simulations of the turbulent flow around and in the wake of MHK turbines. Our goal is to develop general experimental and numerical methodologies to investigate the performance and the fluid dynamics around and in the wake of the HAHT blades. In the first section of this work we present a description of the experimental setup used for performance studies and flow field analysis in the wake of the scale model of the DOE Reference Model 1 turbine, and discuss the preliminary experimental results.

In the second section of this paper, we present the numerical model for characterization of turbine operation and flow field simulation around and in the wake the DOE RM 1 turbine. We present the numerical results at full-scale conditions for performance and flow field characterization under the optimal Tip Speed Ratio ( $TSR = 6.3$ ) and pitch angle ( $\theta_p = 0$ ) that the DOE RM 1 is designed for. These results include the total torque on the turbine blade, 3D lift and drag coefficients on different sections along the blade span and the flow field characterization in the wake of the turbine. The calculated total torque for the above-mentioned  $TSR$  and pitch angle is compared to the corresponding results reported by Lawson et al. [3]. Furthermore, we briefly address and investigate applicability of a second turbulence closure model to performance and flow field characterization of the DOE RM 1.

## EXPERIMENTAL ANALYSIS

### Laboratory Setup

Flume testing was performed with the DOE reference model 1 geometry. The 45:1 scale model consists of a 0.45 m diameter turbine rotor manufactured on a CNC mill from aluminum and a 0.063 x 0.6 m cylindrical nacelle. The nacelle contains a torque sensor (TFF325 Futek, Irvine, California), magnetic encoder (RM22 RLS, Komenda, Slovenia), and permanent magnet

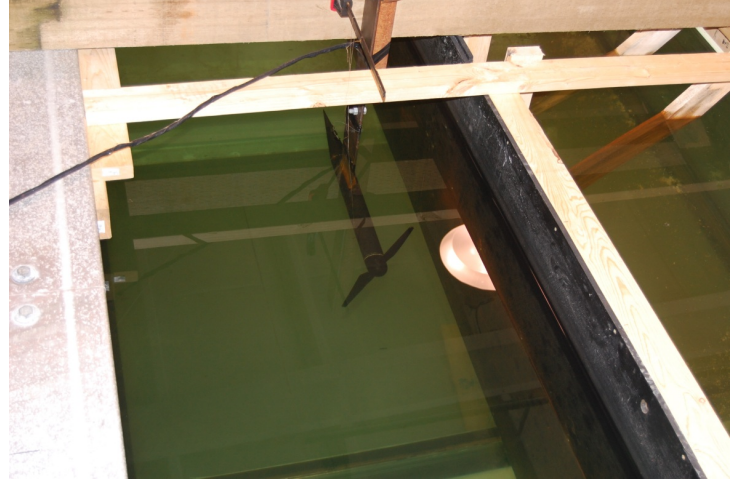


**FIGURE 1.** PHOTOGRAPH OF THE TURBINE MODEL INSIDE THE FLUME.

brake (MC2 Precision Tork, Midland, Michigan) used to apply shaft loading. The torque sensor and magnetic encoder are wired to an analog-digital converter and acquisition system (PCIe-6341 National Instruments, Austin, Texas) sampled at 1000 Hz. The turbine model is mounted to a vertical post extending from the top of the flume to the nacelle. A photograph of the turbine model mounted in the flume is shown in Figure 1.

The experiments were performed at the Bamfield Marine Science Centre, with a 1 m by 12.3 m test section, operating at 0.8 m depth. The blockage ratio was 20%. An ADV (Vector Nortek, Oslo Norway) and PIV (LaVision GmbH., Goettingen, Germany) system were used to characterize the flow upstream from the turbine and in the wake of the turbine. PIV data was taken for 40 seconds at 5 Hz for each imaging location and the results processed in time, under the assumption of statistically steady free stream flow.

### Experimental results

Three model turbines were tested simultaneously for four turbine spacing configurations, as shown in Figure 3. Configurations 1 and 2 consist of three turbines aligned on a common axis in the center of the channel, with a streamwise separation distance of 7 and 5 rotor diameters, respectively. Configurations 3 and 4 consist of turbines with 7 and 5 rotor diameter streamwise separation, respectively, and the upstream and downstream turbines are laterally offset from the middle turbine by 0.5 rotor diameters. Turbines in all configurations were centered in the water column.

An ADV was used to characterize the incoming flow 0.45 m (1D) upstream from the rotor plane at turbine hub depth. In-flow conditions for these tests are an average streamwise velocity of 0.65 m/s and an average turbulence intensity of 12.5%. PIV

images were collected at several locations upstream and downstream of the rotor plane on the rotor centerline as shown in Figure 2. Time-averaged streamwise velocity profiles at three streamwise locations: 0.2 turbine diameters (0.2D) upstream, and 3 and 5 D downstream of the rotor plane were calculated from the PIV measurements. These velocity profiles can be seen

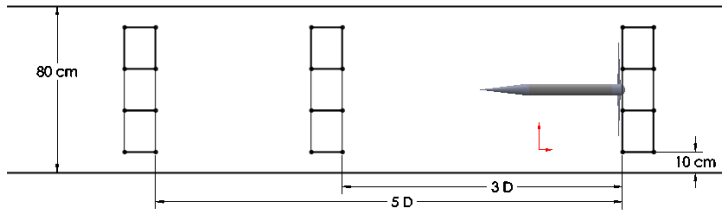


**FIGURE 2.** SCHEMATIC OF PIV INTERROGATION WINDOWS. EACH WINDOW IS 0.2 M DEEP AND 0.15 M WIDE.

in Figure 5; they show the velocity deficit in the turbine wake and the wake recovery downstream.

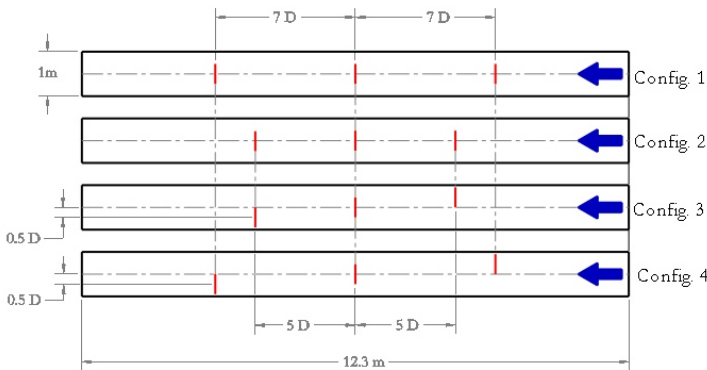


**FIGURE 3.** TOP VIEW SCHEMATIC OF THE FOUR ARRAY CONFIGURATIONS TESTED. THE RED LINES REPRESENT THE TURBINE ROTORS. CONFIGURATIONS 1 AND 2 HAVE THE TURBINES ARRANGED ON A SINGLE AXIS, WITH STREAMWISE SPACING OF 7 TURBINE DIAMETERS AND 5 TURBINE DIAMETERS, RESPECTIVELY. CONFIGURATIONS 3 AND 4 HAVE THE TURBINES ARRANGED WITH 0.5 DIAMETER LATERAL OFFSET BETWEEN TURBINES, AND A STREAMWISE SPACING OF 7 DIAMETERS AND 5 DIAMETERS, RESPECTIVELY.

Turbine performance was characterized for a constant freestream velocity of  $0.59 \text{ m/s}$  across a range of tip speed ratios. The power coefficient is shown in Figure 4, and suggests that the optimum TSR is approximately 9-10. This is higher than the optimum TSR of 7 predicted from the blade element momentum

code, and may suggest a Reynolds number effect, as higher rotational speed create a higher local velocity and therefore higher local Reynolds number.

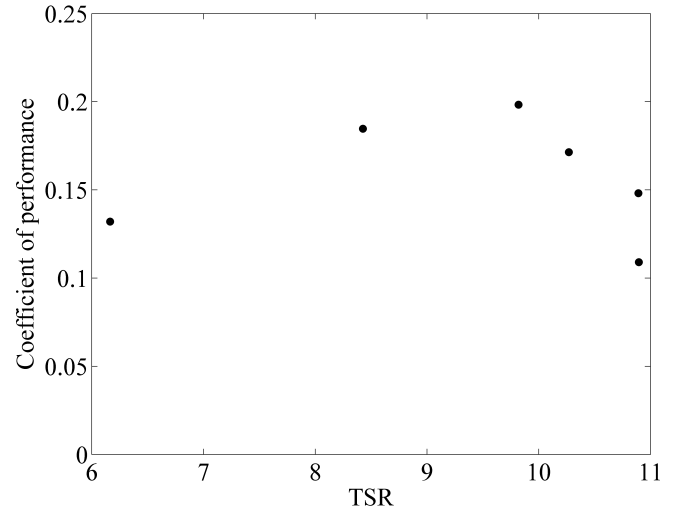


**FIGURE 4.** POWER COEFFICIENT AS A FUNCTION OF TIP SPEED RATIO FOR A SCALED DOWN DOE RM1 TURBINE ( $RE \approx 7 \cdot 10^4$ ).

Power extracted by the three turbines was measured concurrently with the PIV measurements, and is presented in Figure 6. Power measurements from each turbine are normalized by the power extracted by the upstream turbine, in order to elucidate the effect of array spacing on power extraction. The results shown in Figure 6 for configurations 1 and 2 show significantly less power extraction from the middle turbine than the upstream turbine. This is expected, as the velocity incident on the middle turbine has not fully recovered to the freestream velocity. The power extracted by the downstream turbine is greater than that extracted by the middle turbine, which indicates that the combined wake of the upstream and middle turbines recovers velocity more quickly than the wake of the upstream turbine alone. Configurations 3 and 4 have turbines at lateral offset, and show somewhat conflicting power extraction trends. It is expected that the middle turbine in the configurations with lateral offset extract more power than the middle turbines in the axially aligned configurations, but this is only seen in configuration 4. The large power extraction by the downstream turbines in configurations 3 and 4 may indicate a blockage effect, as higher velocity flow is channeled towards one side of the flume.

Turbulence intensity was calculated from the PIV data of an upstream turbine and is shown in Figure 7. Regions of high turbulence intensity from the tips of the rotor are seen at three-ro-

tor diameters downstream of the rotor plane, and the turbulence intensity is seen to diffuse toward the centerline at five rotor diameters downstream. Turbulence intensity increases as the flow encounters each rotor, leading to very high turbulence intensity in the wake of the downstream rotor. High turbulence intensity promotes the diffusion of momentum, which may be responsible for the increased rate of momentum recovery in the wake of the downstream turbine.

## NUMERICAL SIMULATIONS

### Simulation Setup

We use a Single Reference Frame (SRF) implementation of the DOE RM 1 turbine with the RANS equations to study the flow field around and in the wake of this HAHT turbine blade. The SRF model renders the unsteady problem of flow around a turbine blade in a fixed reference frame into a steady problem of flow with respect to the rotating reference frame moving with the blade. In this formulation, the effect of rotation is input into the equations of fluid motion by adding body forces that represent the inertial effects associated with the centrifugal and Coriolis accelerations [4]. This allows the equations to be integrated using a stationary grid and to avoid the complexity and stiffness associated with rotating mesh simulations. The trade off in using this model is that it requires an axisymmetric domain and periodic boundary conditions.

Figure 8 shows the computational domain for the SRF model. Taking advantage of the DOE RM 1 turbine symmetry (two bladed rotor), only half of the domain is modeled in this work. The boundary condition at the inlet is a constant velocity and at the outlet is a uniform pressure. Cyclic-periodic boundaries are prescribed on the symmetry plane of the domain to simulate the blade rotation. The domain's top cylindrical boundary sets the limit of the computational domain. The distance between this boundary and tip of the turbine blade is about 23 m that result into a small blockage ratio of 6%. This boundary is modeled with a slip free boundary condition. The close-up of the turbine blade section in figure 8 shows that the span of the blade is divided into small sections to calculate 3D lift and drag coefficients at each section along the blade. Including the actual geometry of the blade in this model provides the opportunity to capture the details of the flow field in the near wake region. The following section discusses some of the numerical results obtained from these simulations.

### Flow Field on the Blade Surface

Pressure and streamlines on the DOE RM 1 blade are shown in figure 9. The pressure fields on the pressure (left) and suction (right) sides of the blade are simulated using two different turbulence closure models, SST  $k - \omega$  and SA. In this figure the pressure contours are superimposed by the limited streamlines

along the blade.

The SST  $k - \omega$  is a well-developed two-equation turbulence closure model that has been extensively used for the flow field investigation around and in the wake of the wind and hydrokinetic turbines. The Spalart-Allmaras (SA) is a one-equation turbulence model, in which it is not necessary to calculate a length scale related to the local shear layer thickness. This fact makes SA computationally less expensive and more robust. The SA model is designed specifically for external aerodynamics applications involving wall-bounded flows and has been shown to give good results for boundary layers subjected to adverse pressure gradients. Therefore, it is a good candidate for application to the simulation of the flow field on hydrokinetic turbine blades, which have core similarities with the fluid mechanics around wings and wind turbine rotors. We observe differences in the modeled pressure and velocity field along the DOE RM 1 blade span using  $k - \omega$  and SA turbulence closure model. These result in different lift and drag coefficients that ultimately lead to different power predictions, as will be discussed below.

As seen in figure 9 the simulated pressure field and limited streamlines on the pressure side of the blade using two turbulence models,  $k - \omega$  and SA, look similar to each other. However, in the simulated pressure field via the SST  $k - \omega$  model on the suction side of the blade the region of negative pressure, visualized by dark blue transitioning to light green color (i.e. range of -80 to -30 kPa), is larger than the corresponding region simulated by the SA model. The reason behind this goes back to the difference in the formulation of the two turbulence closure models (one-equation versus two-equation) and the difference in the approximation that they use to model the turbulent boundary layer close to the blade wall using variables in the turbulent flow (modified turbulent kinematic viscosity,  $\tilde{\nu}$ , versus turbulent kinetic energy and specific dissipation,  $k$  and  $\omega$ ). The SA model equates the value of the modified turbulent viscosity,  $\tilde{\nu}$ , to zero at the blade wall and it assumes that the centroid of the wall-adjacent cell falls within the logarithmic region of the boundary layer. Then, it uses the wall function approximation to evaluate the velocity and the modified turbulent viscosity in the near wall region. However, in the SST  $k - \omega$  model the estimated value of the boundary layer velocity based on the wall function approximation is used to evaluate values of the  $k$  and  $\omega$  based on different empirical relations to model the turbulent boundary layer in this region.

The larger negative pressure region on the suction side of the blade simulated using the SST  $k - \omega$  model results into larger lift and smaller drag forces along that section of the blade span. This observation is consistent with the higher values of lift and smaller values of drag coefficients predicted by the SST  $k - \omega$  model compared to the SA model, shown in figure 10 and discussed below. Presented also below, table 2 shows the calculated power in the simulation using the SA model is about 35% lower than the prediction with the SST  $k - \omega$  model.

Once we have a clear understanding of the flow field on the rotor blade surfaces, we analyze the evolution of the 3D lift and drag coefficients on different sections along the blade span, computed from these RANS simulations. These values are compared with Xfoil calculations that are routinely used in the absence of experimental data, for Blade Element Model calculations in design and performance/wake studies.

Figure 10 shows values of angle of attacks (AOAs) (left y-axis) and values of the lift and drag coefficients (right y-axis) along the blade span ( $x$ -axis). In this figure there are three sets of the lift and drag coefficients curves, which are calculated using different numerical approaches: The red curves with triangles on top are the lift and drag coefficients calculated by the 3D RANS with SA as the turbulence closure model. The blue curves superimposed with star symbols represent the lift and drag coefficients from the 3D RANS simulation with  $k-\omega$  as the turbulence closure model. Finally the black curves with circles on top show the lift and drag coefficients calculated based on a 2D potential flow model (Xfoil). The green curve in this figure shows the values of AOAs, which are the almost identical in both of the 3D RANS simulation with different turbulence closure model.

As seen in figure 10 values of AOAs are monotonically decreasing moving from the blade root towards the tip. Parallel to the decrease of the AOA values toward the blade tip, the lift coefficients simulated by all three models decrease as well. Noticeable here is a rapid decrease in the values of the 3D lift coefficients at the region close to the blade tip. This rapid change is associated with the formation and shedding of the tip vortex that reduce the lift well below the equivalent two-dimensional value. Since this signature of the flow field is not captured in the 2D simulations, the calculated 2D lift coefficients are almost constant in this region and do not match the decay trend of the 3D lift coefficients.

Moving from the root toward the mid-span of the blade there is a good agreement between the calculated 2D and 3D lift coefficient using the SA closure model. In this part of the blade, the flow field around each section evolves in a plane perpendicular to the blade axis, and thus is well represented by the assumption of an infinite span airfoil section underlying the 2D simulations. Under these circumstances, the three dimensionality of the flow field does not affect the resultant lift force on the blade sections. The calculated 2D and 3D (SA model) lift coefficients are in a good agreement with each other.

Approaching the root of the blade the shape of the DOE RM 1 blade airfoil cross sections transitions from a hydrodynamic shape to a semi-elliptical shape. With this geometrical transition, the flow field starts to separate from these sections. The small region of separated flow visualized by the streamlines on the suction side of the blade at the trailing edge of the blade root confirms this hypothesis. Observation of stiff convergence trend in the 2D simulations for the last few sections showed the limitation of the 2D simulation for calculation of the lift coefficient

values in these sections. As a result of this, the 2D and 3D lift coefficient values start to disagree approaching the root of the blade. We should highlight that the similar decay trend between the 3D lift coefficient values from  $k-\omega$  and SA models (red and blue curves) makes the above comparisons between 2D and 3D lift coefficients valid for both cases. However, as seen in the figure 10 the values of the lift coefficients calculated in simulations with the SST  $k-\omega$  model are larger than the corresponding values calculated by the SA model. The reason for this difference goes back to the difference in formulation of the SST  $k-\omega$  and SA models that will be discussed in the next subsection.

Finally, the last area of discrepancy between the 2D and 3D coefficients lies in the value of drag coefficients. As seen in figure 10 the trend of the drag coefficients variation along the blade span is similar in all three cases. The values of the 2D and 3D drag coefficients calculated by the SST  $k-\omega$  model are very close to each other. However, the 3D drag coefficients calculated from the simulation with the SA turbulence closure model are higher than the values from Xfoil and the 3D simulation with the SST  $k-\omega$  turbulence model.

The lift and drag coefficients as a function of angle of attack derived from these simulations can be used in models based on the Blade Element Theory (BET). These provide a simpler representation of MHK turbines, with lower computational cost. More accurate values of the lift and drag coefficients (i.e. from fully 3D RANS simulations instead of potential 2D codes) for the lower fidelity models lead to more accurate results, without increasing the low computational time and cost that make these BET models well-suited for large-scale studies of MHK turbines.

### Flow Field in the Near Wake (3D RANS using SST $k-\omega$ model)

After a detailed discussion about the lift and drag forces variation along the DOE RM 1 turbine blade span, we move into the turbine blade downstream and investigate the fluid dynamics in the near wake region of this turbine blade. Figure 11 shows the streamwise velocity contours normalized with the free stream velocity. These contours are plotted on planes perpendicular to the flow direction along the SRF computational domain. The sequence of these planes starts at  $0.25R$  turbine upstream (top left plot), and moves to  $2.5R$  downstream (bottom right plot). As we move downstream in figure 11, the flow starts to decelerate as it approaches the turbine blade. At the location of the blade ( $Y/R = 0$ ) acceleration of the flow on the suction side of the blade, deceleration on the pressure side, and tip vortex shedding from the blade tip are clearly observed. As the distance downstream from the turbine increases, the tip vortices become diffuse (the high speed signature from both can be seen at  $Y/R=0.25$ ) and break down. Furthermore, the velocity contour in the wake becomes more homogeneous, such that at about  $1.5R$  downstream of the blade, the streamwise velocity in the wake becomes axisymmetric

ric. As discussed before, the SRF model is capable of capturing the details of the flow field close to the blade. This provides the opportunity of detailed comparison between numerical and experimental data. Furthermore, observation of the axisymmetric wake beyond 1.5R downstream the blade justifies the use of less computationally intensive models based on BET, such as BEM, to study the physical phenomena that are dominated by the far wake of the turbine. Turbine array optimization and the effect of operating turbines on the sedimentation process of suspended particles in a MHK sites are two examples of these types of studies.

### Flow Field in the Far Wake (3D RANS using SST $k - \omega$ model)

Figure 12 shows the streamwise velocity contours normalized with the free stream velocity on a plane parallel to the free stream direction across the centerline of the channel in the SRF computational domain. Velocity profiles along the radial direction are superimposed over the color contours. These show the velocity deficit at different distances downstream of the blade. As the flow moves from left to right and approaches the blade, it decelerates. This is visualized by the transition from orange to yellow and green in the velocity contours. The blade extracts momentum from the incoming flow and generates a turbulent wake. This region is shown by colder colors in the wake of the blade. The captured vortex shedding at the blade tip is visualized in the form of small, discrete high-speed blobs near the tip of the blade, corresponding with the high velocity in the core of the tip vortices. Vortices are stronger closer to the blade, and get weaker as they travel about one radius downstream, where the vorticity diffuses and eventually disappears in the flow. The velocity deficit in the wake are visualized by dotted black lines at different positions downstream of the blade. The maximum deficit happens in the region close to the blade. Farther downstream, the velocity profiles recover as the wake entrains high velocity flow from the undisturbed surrounding fluid.

### Comparison of Computational Results across CFD Solvers and Turbulence Closure Models (SST $k - \omega$ and SA).

Since the DOE RM 1 is a newly developed reference model, there is a lack of publicly available data on the flow field around this rotor design. Lawson et al. [3], from the National Renewable Energy Laboratory (NREL), is the only currently available reference on the DOE RM 1. In order to build confidence on the predictive capabilities of numerical simulations, we compare our results against those published results [3]. The operating conditions (i.e. the TSR, turbulent intensity and working fluid), numerical settings (i.e. turbulence closure model) and the computational domain mesh resolution from two simulations were matched with each other, in order to make this comparison mean-

**TABLE 1.** COMPARISON BETWEEN TWO DIFFERENT NUMERICAL APPROACHES FOR CHARACTERIZATION OF THE DOE RM 1 HAHT IN THE NREL AND NNMREC.

Research Group	NREL	NNMREC
Numerical Solver	STAR CCM+	FLUENT 12.0
Turbulence Model	SST $k - \omega$	SST $k - \omega$
Mesh Structure	Unstructured	Structured
Element type	Polyhedral	Brick
Torque [N-m]	$2.13 \times 10^5$	$2.16 \times 10^5$
Relative Difference [%]	0	1.41

**TABLE 2.** COMPARISON BETWEEN THE CALCULATED TOTAL POWER OF THE DOE RM 1 HAHT USING DIFFERENT TURBULENCE MODELS UNDER MATCHED OPERATION CONDITIONS ( $V_\infty=1.9$  m/s and  $\omega=11.5$  rpm) AND GRID RESOLUTION.

	Power [kW]	Relative Diff. [%]
NREL (SST $k - \omega$ )	511.2	-
NNMREC (SST $k - \omega$ )	518.4	1.41
NNMREC (SA)	330.9	35.27

ingful. Table 1 shows the relevant data from the two numerical approaches.

We observe that the difference between the values of estimated total torque (for each blade) for the DOE RM 1 reported by Lawson et al. at NREL and our numerical results at NNMREC is less than 1.5%. This is remarkably close agreement, considering the exclusion of a small section of the root (about 50 cm) and the turbine nacelle in our model and the differences between two numerical simulations such as using two different numerical solvers, mesh structures and element types.

We should highlight that in the comparison presented in table 1 both of the numerical approaches (at NREL and NNMREC) used the SST  $k - \omega$  turbulence closure model with the RANS simulations. Table 2 shows the comparison between the calculated power using 3D RANS simulation with the  $k - \omega$  and SA as the turbulence closure model. The calculated power from the two numerical approaches in the NREL and NNMREC with matched operating conditions and numerical models (i.e. SST  $k - \omega$ ) are in a good agreement with each other.

Noticeable in table 2 is the value of the calculated power from 3D RANS simulation with the SA as the turbulence closure model. As seen in this table the value of the calculated power

in this simulation is about 35% lower than the calculated power with the SST  $k - \omega$  model. The root of this large discrepancy in the predicted torque and power lies in subtle differences in the flow field on the blade surface which, as shown previously, can be traced to the formulation of the two turbulence closure models (one-equation versus two-equation) and the approximation they use to model the turbulent variables close to the blade wall. The above-mentioned differences between the two models result in different simulated resultant lift and drag forces along the blade span, hence differences in the calculated power values. At this stage of the research and development on the DOE RM 1, the scarcity of experimental results makes a detailed comparison between simulations and experiments difficult, and therefore a complete assessment of the capabilities and weaknesses of these two turbulence models is still pending for use in MHK turbine design and performance analysis. The observation of the gap in the calculated power via the  $k - \omega$  and SA models, however, and the accurate results from RANS simulations using the SA model in previous studies on wind turbines makes this an interesting problem to investigate. Providing a better understanding of capabilities and limitations of the each of these models can help us to reduce computational cost and time and increase the stability and accuracy in the flow field investigation and performance characterization of the DOE RM 1 and other hydrokinetic turbines designs.

## CONCLUSIONS

We have performed numerical simulations of the full scale DOE RM1 and experiments on a 45:1 scale geometrically-similar model of the DOE RM1 rotor in a large flume. The numerical simulations compared well with previous RANS-based computations of the DOE RM1 turbine. Simplification in the hub and blade root geometry did not significantly impact performance and flow field predictions. Selection of turbulence closure models for the RANS simulations has significant impact on results, with more work to justify differences and to guide model construction necessary to bring this methodology to design. 3D lift and drag coefficients obtained from high fidelity simulations can be used in simpler Blade-Element method simulations for large domain, multiple turbine simulations. Strong Reynolds number effects in the experimental results precluded the direct comparison with CFD predictions. Turbine redesign to avoid that limitation, as well as computations with scale down models will close this experimental/numerical gap in the near future.

## REFERENCES

[1] Batten, W., Chaplin, J., Bahaj, A., and A., M., 2007. "Experimentally validated numerical method for hydrodynamic design of horizontal axis tidal turbines." *Ocean Engineering*, **34**, p. 1013.

- [2] Batten, W., Chaplin, J., Bahaj, A., and A., M., 2008. "The prediction of the hydrodynamic performance of marine current turbines." *Renewable energy*, **33**, p. 1085.
- [3] Lawson, M., Li, Y., and Sale, D., 2011. "Development and verification of a computational fluid dynamics model of a horizontal-axis tidal current turbine". In Proceedings of the 30th International Conference on Ocean, Offshore, and Arctic Engineering.
- [4] Warsi, Z., 1993. *Fluid Dynamics, Theoretical and Computational Approaches*. CRC Press.

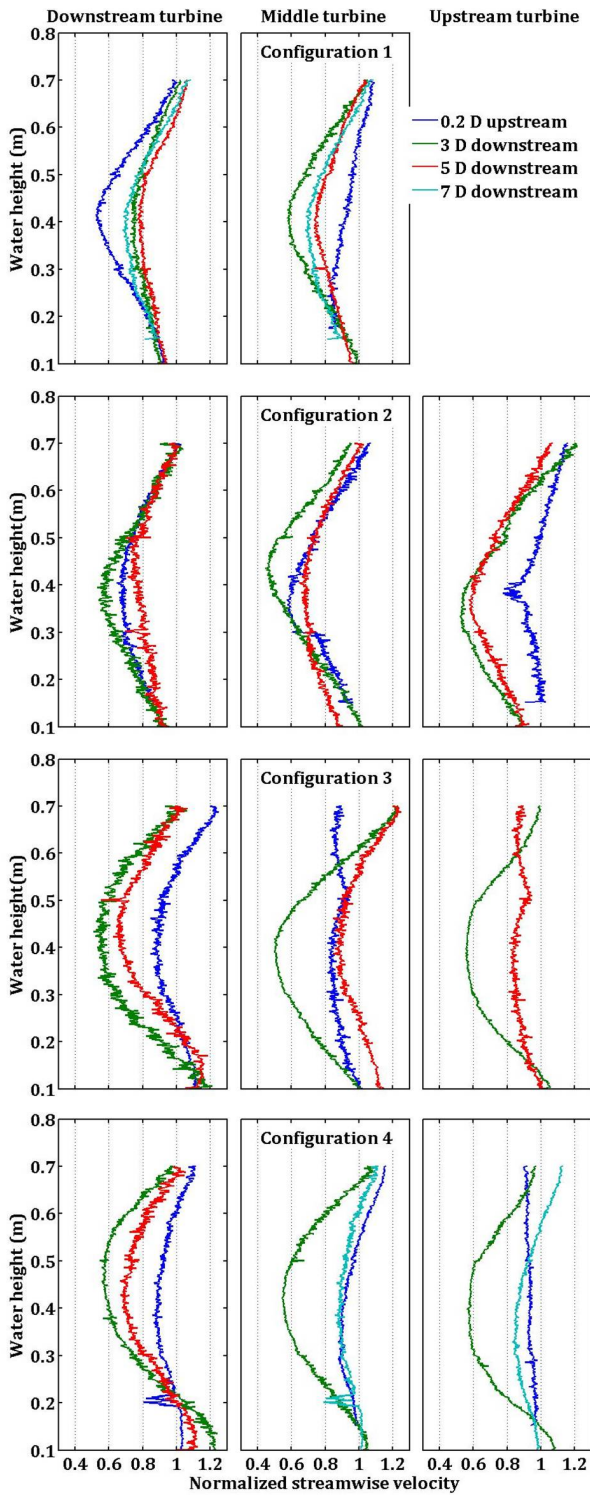


**FIGURE 5.** TIME-AVERAGED STREAMWISE CENTERLINE VELOCITY PROFILES.

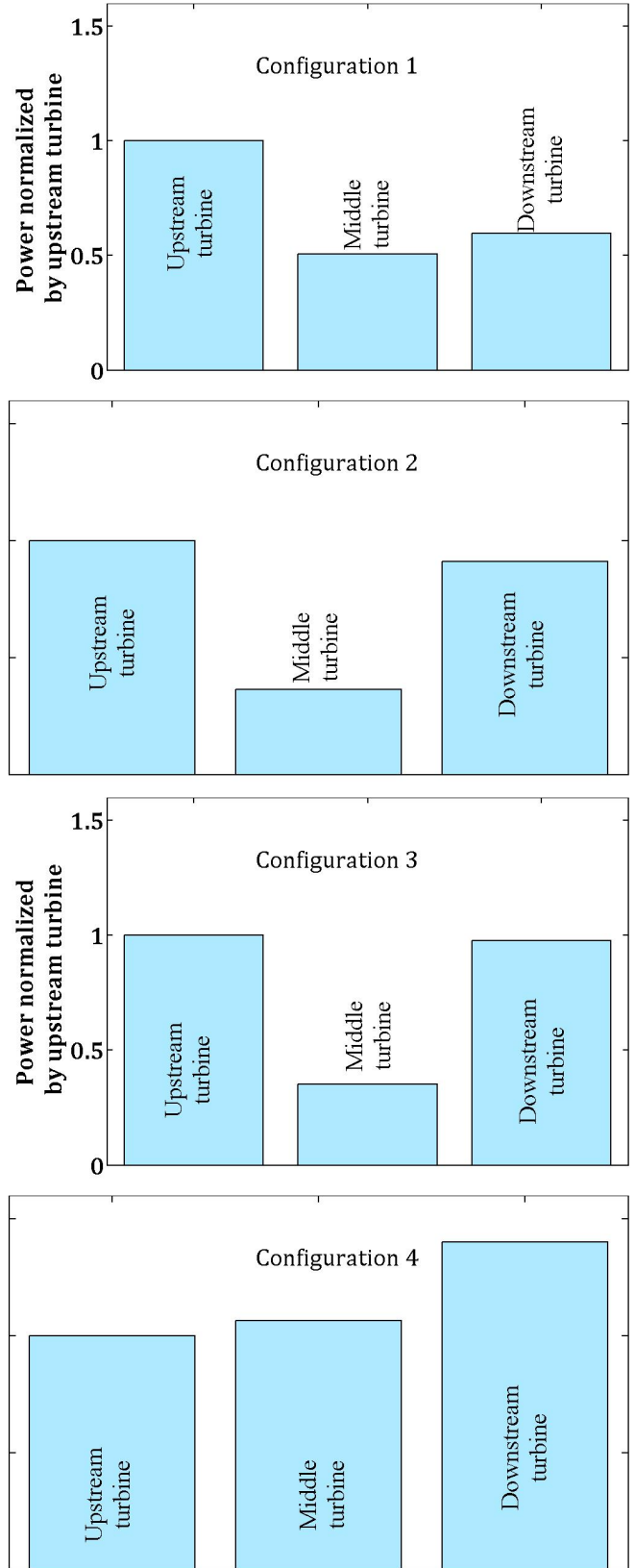


**FIGURE 6.** AVERAGE POWER EXTRACTED BY EACH TURBINE, NORMALIZED BY THE POWER EXTRACTED BY THE UPSTREAM TURBINE, FOR ARRAY CONFIGURATIONS 1-4.

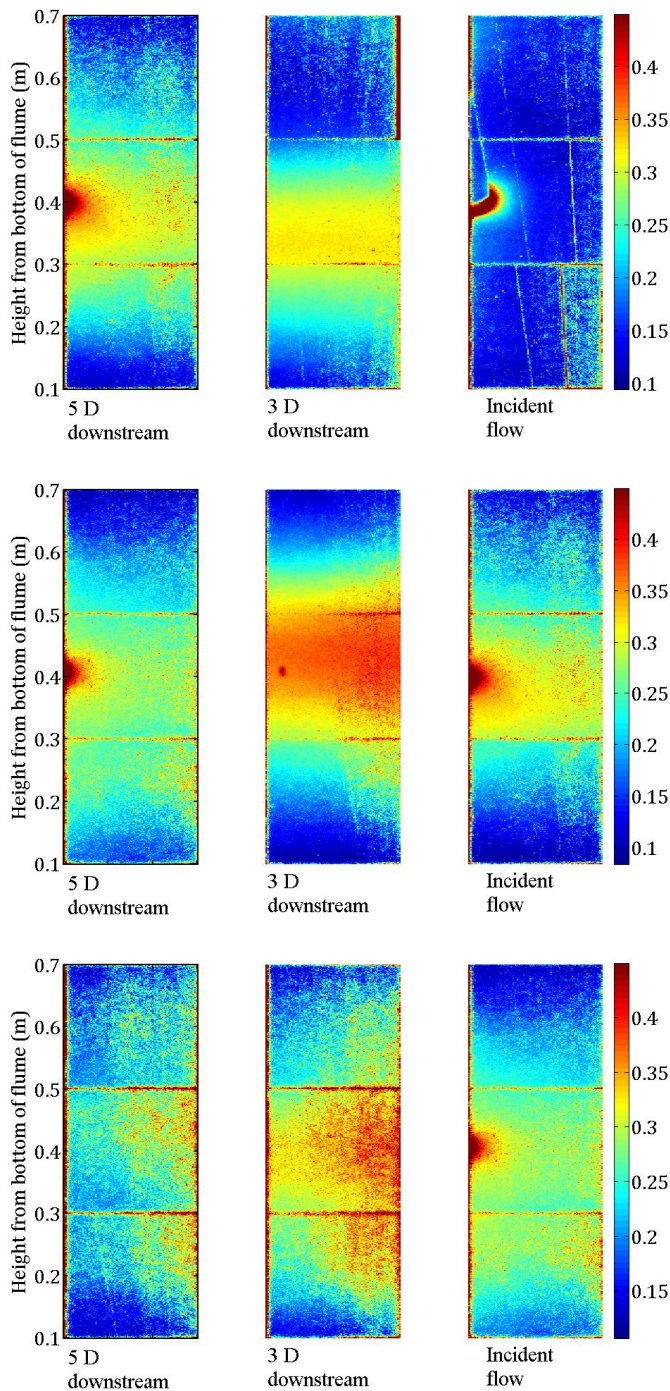


**FIGURE 7.** TURBULENCE INTENSITY IN THE WAKES OF THE UPSTREAM (TOP), MIDDLE (MIDDLE), AND DOWSTREAM (BOTTOM) TURBINES ARRANGED IN CONFIGURATION 2.

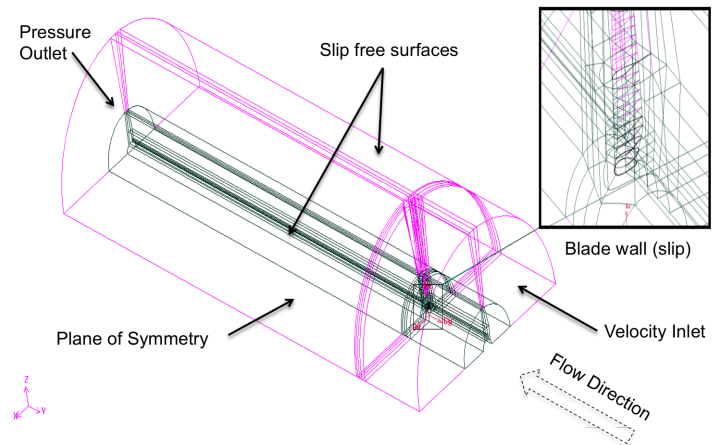


**FIGURE 8.** COMPUTATIONAL DOMAIN AND BOUNDARY CONDITIONS USED WITH THE SRF MODEL. THE ACTUAL GEOMETRY OF THE DOE RM 1 BLADE (ZOOMED IN SECTION) IS INCLUDED IN THIS COMPUTATIONAL DOMAIN.

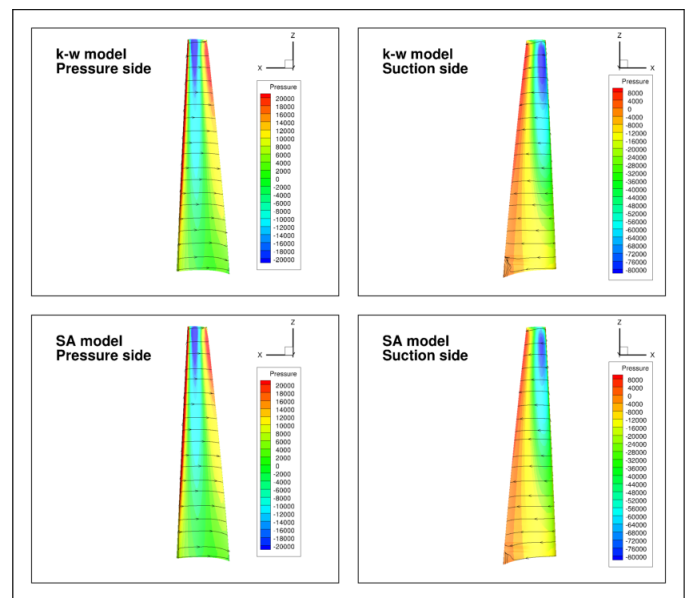


**FIGURE 9.** COMPARISON BETWEEN THE SIMULATED PRESSURE FIELD ON THE PRESSURE AND SUCTION SIDE OF THE DOE RM 1 BLADE USING  $k - \omega$  AND SA TURBULENCE CLOSURE MODELS.

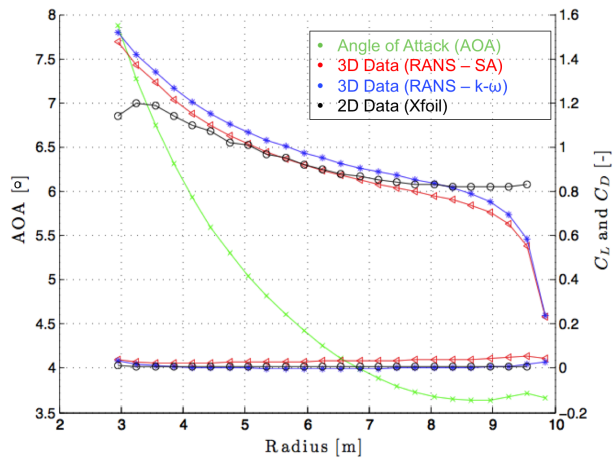


**FIGURE 10.** 2D and 3D LIFT AND DRAG COEFFICIENTS FOR THE DOE RM 1 BLADE SPAN OPERATING IN  $TSR=6.3$  AND REYNOLDS NUMBER OF  $\approx 10^6$  BASED ON THE AVERAGE CHORD LENGTH ALONG THE BLADE SPAN.

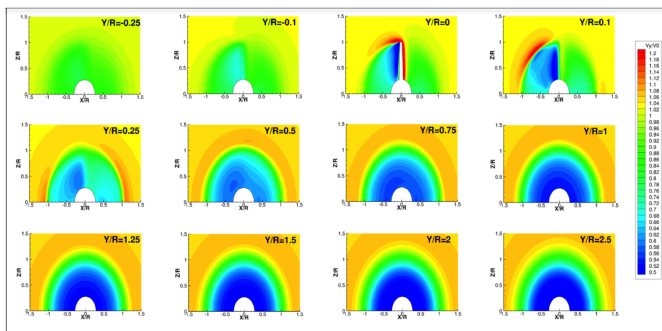


**FIGURE 11.** NORMALIZED STREAMWISE VELOCITY CONTOURS ON THE Y-CUTS PLANE ALONG CHANNEL FOR DOE RM 1 TURBINE SIMULATED WITH THE SST  $k - \omega$  TURBULENCE CLOSURE MODEL.

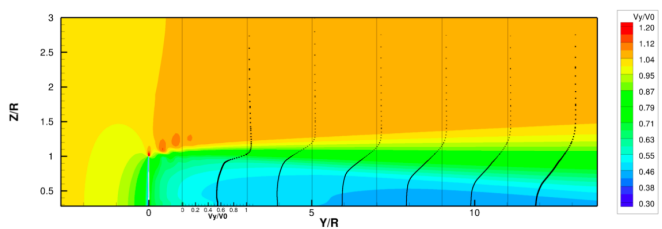


**FIGURE 12.** VELOCITY CONTOURS AND VELOCITY DEFICIT PROFILES IN THE TURBULENT WAKE SIMULATED WITH THE SST  $k - \omega$  TURBULENCE CLOSURE MODEL.